



Contents lists available at ScienceDirect

Journal of Biomechanics

journal homepage: [www.elsevier.com/locate/jbiomech](http://www.elsevier.com/locate/jbiomech)  
[www.JBiomech.com](http://www.JBiomech.com)

## Full-field measurement of micromotion around a cementless femoral stem using micro-CT imaging and radiopaque markers

V. Malfroy Camine<sup>a</sup>, H.A. Rüdiger<sup>b,c</sup>, D.P. Pioletti<sup>a</sup>, A. Terrier<sup>a,\*</sup>

<sup>a</sup> Laboratory of Biomechanical Orthopedics, Ecole Polytechnique Fédérale de Lausanne, Station 19, 1015 Lausanne, Switzerland

<sup>b</sup> Service of Orthopedics and Traumatology, Lausanne University Hospital, Lausanne, Switzerland

<sup>c</sup> Department of Orthopedic Surgery, Schulthess Clinic, Zürich, Switzerland

### ARTICLE INFO

#### Article history:

Accepted 21 October 2016

#### Keywords:

Primary stability  
Micromotion  
Femoral stem  
Micro-CT  
Total hip replacement

### ABSTRACT

A good primary stability of cementless femoral stems is essential for the long-term success of total hip arthroplasty. Experimental measurement of implant micromotion with linear variable differential transformers is commonly used to assess implant primary stability in pre-clinical testing. But these measurements are often limited to a few distinct points at the interface. New techniques based on micro-computed tomography (micro-CT) have recently been introduced, such as Digital Volume Correlation (DVC) or markers-based approaches. DVC is however limited to measurement around non-metallic implants due to metal-induced imaging artifacts, and markers-based techniques are confined to a small portion of the implant. In this paper, we present a technique based on micro-CT imaging and radiopaque markers to provide the first full-field micromotion measurement at the entire bone-implant interface of a cementless femoral stem implanted in a cadaveric femur. Micromotion was measured during compression and torsion. Over 300 simultaneous measurement points were obtained. Micromotion amplitude ranged from 0 to 24  $\mu\text{m}$  in compression and from 0 to 49  $\mu\text{m}$  in torsion. Peak micromotion was distal in compression and proximal in torsion. The technique bias was 5.1  $\mu\text{m}$  and its repeatability standard deviation was 4  $\mu\text{m}$ . The method was thus highly reliable and compared well with results obtained with linear variable differential transformers (LVDTs) reported in the literature. These results indicate that this micro-CT based technique is perfectly relevant to observe local variations in primary stability around metallic implants. Possible applications include pre-clinical testing of implants and validation of patient-specific models for pre-operative planning.

© 2016 Elsevier Ltd. All rights reserved.

### 1. Introduction

During the past two decades, the number of cementless hip arthroplasties has increased significantly from 13,650 procedures in 2003 to 27,031 in 2014 (Australian Orthopaedic Association National Joint Replacement Registry, 2015), and it is now the preferred type of fixation for patients under 70 years old.

However, the cumulative revision rate at 14 years reaches 8% and aseptic loosening remains among the most common causes for revision of cementless femoral components. For this reason, improving the long-term success of cementless femoral stems continues to be a major focus in the field of total hip arthroplasty.

A good primary stability of the implant is widely recognized as the most important factor for a successful cementless hip

arthroplasty. Primary stability is characterized by the amount of relative bone-implant micromotion at the interface, right after implantation and before osseointegration takes place. Many researchers have reported that excessive implant micromotion leads to fibrous tissue formation and failed bone ingrowth (Engh et al., 1992; Pilliar et al., 1986; Søballe et al., 2009).

Much research in the recent years has focused on measuring bone-implant micromotion for the pre-clinical testing of implants. An optimal experimental micromotion measurement technique for the pre-clinical testing of femoral stems should be able to evaluate micromotion at every point of the bone-implant interface while having a bias below 10  $\mu\text{m}$  (Viceconti et al., 2000). Considering the maximum micromotion still allowing osseointegration is around 100  $\mu\text{m}$ , this bias value would represent a relative error of 10%. Current techniques available to measure implant micromotion rely mostly on linear variable differential transformers (LVDTs) (Enoksen et al., 2014; Fottner et al., 2009; Kassi et al., 2005; Monti et al., 1999; Pettersen et al., 2009; Østbyhaug et al.,

\* Corresponding author.

E-mail address: [alexandre.terrier@epfl.ch](mailto:alexandre.terrier@epfl.ch) (A. Terrier).

2010). Despite their excellent accuracy, they allow only a handful of simultaneous measurement points. Finite element (FE) modeling is another popular method to estimate micromotion of cementless stems. It provides information on local micromotion and can be used for the pre-clinical testing of implants (Abdul-Kadir et al., 2008; Bah et al., 2015; van der Ploeg et al., 2011; Viceconti et al., 2006) as well as for patient-specific pre-operative planning (Pettersen et al., 2009; Reggiani et al., 2007). But experimental validation of FE models predictions remains challenging, restraining a more extensive use of these models in clinical practice (Taylor and Prendergast, 2015). More recently, micromotion measurement techniques based on micro-computed tomography (micro-CT) imaging were introduced, and demonstrated great potential. Notwithstanding the very high number of measurement points they can collect, they were limited to measurement around non-metallic implants due to imaging artifacts (Sukjamsri et al., 2015) or confined to a small portion of the implant (Gortchacow et al., 2012, 2011).

In the present study, we extend a micromotion measurement technique based on radiopaque markers and micro-CT imaging (Gortchacow et al., 2011) to measure three dimensional micromotion at the entire bone-implant interface of a cementless femoral stem implanted in a cadaveric femur. The method will allow to measure micromotion for axial compression and torsion. Our objective is to guarantee a bias inferior to 10  $\mu\text{m}$  and a good repeatability to enable rigorous pre-clinical testing of cementless implants primary stability.

## 2. Method

### 2.1. Cadaveric femur and femoral stem preparation

A left human cadaveric femur, formalin-fixed, was prepared for implantation by a senior orthopedic surgeon. The surgeon performed femoral neck osteotomy and femoral broaching according to the recommendations of the implant's manufacturer. After broaching, around 1000 stainless steel spherical markers of diameter 600  $\mu\text{m}$  (MPS Micro Precision Systems AG, Biel, Switzerland) were manually press-fitted on the endosteal surface of the femoral canal and the cancellous bone of the metaphysis using a spatula. Appropriate care was taken to get a uniform distribution of bone markers in the canal (Fig. 1).

A collared, straight cementless femoral stem with a standard offset neck (Corail<sup>®</sup> Hip System, size 11, DePuy Synthes Joint Reconstruction, Warsaw, IN, USA) was selected for implantation. The stem is made of forged titanium alloy (TiAl6V4) and is fully coated with 155  $\mu\text{m}$  of hydroxyapatite. To facilitate the accommodation of the bone-implant construct inside the experimental setup, the stem femoral neck was cut 27 mm medial and parallel to the implant extraction threaded hole axis. 30 tantalum spherical markers of diameter 800  $\mu\text{m}$  (X-medics Scandinavia, Frederiksberg, Denmark) were glued (Loctite 401, Loctite Corporation, Dublin, Ireland) on the stem surface, within drilled holes of 1 mm depth and 850  $\mu\text{m}$  diameter (Fig. 1). The surgeon then proceeded to the femoral stem insertion in the broached femur.

### 2.2. Loading devices

Two custom loading devices were developed to apply axial compression and torsion on the stem. The loading devices had to fit inside a micro-CT scanner and had to be sufficiently permeable to X-ray. Each device was composed of two parts: the loading system and the sample holder, enclosed in a 2 mm thick tube made of 6060 aluminum alloy (Fig. 1).

The compression device was modified from an existing one (Gortchacow et al., 2012). The distal part of the femur was cut away at approximately 220 mm from the tip of the greater trochanter. A template was used to pot the distal femur and ensure its alignment (load axis along stem axis) inside the device, using the stem extraction threaded hole. The femur was distally potted with epoxy resin (Neukadur Multicast 20, Altropol Kunststoff GmbH, Stockelsdorf, Germany), 30 mm away from the distal end of the stem. Minimal reaming of the surface of the greater trochanter laterally (2–3 mm) was performed to enable proper fitting inside the device. The applied load was monitored by a load cell (LCM202-5KN, Omega Engineering, Inc., Stamford, CO, USA).

The torsion device applied an axial torsion on the bone-stem system. The proximal part of the stem was restrained by a clamping system. The stem extraction threaded hole was used to ensure stem alignment along the torsion axis. The stem neck was clamped by two steel cone point screws. The distal femur and the proximal clamping system were potted with epoxy resin inside a template, before insertion in the device. A torsion was applied to the distal femur through a rotary shaft driven by a worm gear. The torque was monitored by a reaction torque cell (TQM301-45N, Omega Engineering, Inc., Stamford, CO, USA).

### 2.3. Micro-CT scanning protocol

To measure micromotion, the bone-implant interface was first scanned during loading and then after loading with a micro-CT scanner (Skyscan 1076 *in vivo* micro-CT, Bruker micro-CT, Kontich, Belgium). These two scans are referred to hereafter as loaded scan and unloaded scan correspondingly. The acquisition parameters for the

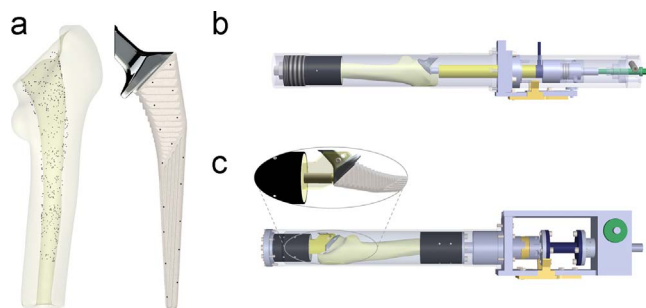


**Fig. 1.** Experimental setup. (a) Bone markers spread inside the femoral canal (left). Stem neck cut and implant markers stuck on implant surface (right). (b) Compression loading device. The distal femur is cemented (black). Compression is applied through a cylinder (yellow) driven by a screw jack (green) and is controlled by a load cell (blue) (c) Torsion loading device. The proximal stem is restrained by a clamping system (yellow). The proximal stem and the distal femur are cemented (black). Torsion is applied through a worm gear (green) and is controlled by a torque sensor (blue). (For interpretation of the references to color in this figure legend, the reader is referred to the web version of this article.)

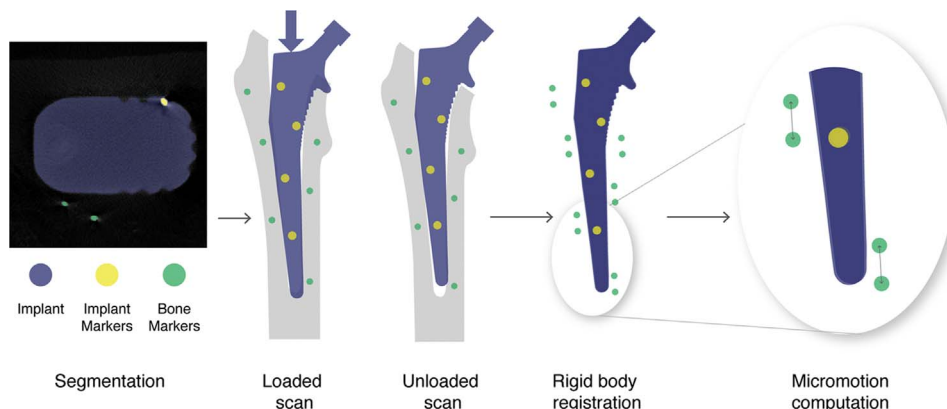


**Fig. 2.** Image processing and micromotion computation. Bone and implant markers are segmented on micro-CT scans. Implant markers from the loaded scan are superimposed to implant markers from the unloaded scan. Micromotion is the displacement between corresponding bone markers from the registered loaded scan to the unloaded scan.

scans were the following: 1 mm aluminum filter, voltage 100 kV, current 100  $\mu$ A, exposure time 310 ms, rotation step 0.7°, 360° scanning, scanning width 68 mm, and frame averaging 2. The scanning length was 21 mm. To cover the whole implant length, 7 scans at different positions along the stem were combined by moving the motorized sample's stage accordingly. Scanning duration for one 21 mm scan was 24 min, resulting in 170 min of scanning to cover the whole stem. Scans were then reconstructed to a final isotropic voxel size of 35  $\mu$ m (NRecon v 1.6.10.4, Bruker micro-CT, Kontich, Belgium). A ring artifact correction of level 4 and a beam hardening correction of 20% were applied to improve the image quality.

#### 2.4. Image processing and micromotion computation

The reconstructed images were processed in Amira (Amira v6.0.1, FEI, Hillsboro, OR, USA). Segmentation of bone and implant markers was completely automatized, using the difference in size and radiopacity of bone and implant markers (Fig. 2). The centroids of all markers were extracted and filtered by size to eliminate noise and clusters of contiguous markers.

Micromotion analysis was performed by a custom algorithm (Matlab r2016a, The Mathworks, Inc., Natick, MA, USA). The loaded and unloaded scans did not share the same coordinate system. The coordinate system of the unloaded scan was used as a reference. The implant was considered rigid so that the coordinate systems of both scans could be aligned using rigid body registration. The correspondence between implant markers in the loaded and unloaded scans was found using an iterative closest point (ICP) algorithm (Besl and McKay, 1992). The rigid transformation matrix between the loaded and unloaded scans was then computed, and applied to all markers from the loaded scan, so that in the end, all markers from the loaded and unloaded scans were in the same coordinate system.

Micromotion was defined as the three dimensional displacement between corresponding loaded and unloaded bone markers. The correspondence between bone markers was computed with the ICP algorithm. Mismatched markers were then eliminated using median absolute deviation to remove outliers (Leys et al., 2013). The micromotion vector was separated into components tangential and normal to the stem surface. Micromotion was then interpolated using natural neighbor interpolation and displayed on the stem surface.

#### 2.5. Micromotion measurement in compression and torsion

For compression testing, a load of 1800 N was applied on the stem. The load was chosen according to the average load during walking measured with instrumented hip implants (Bergmann et al., 2010a, 2010b). The bone was preconditioned with 50 compressive load cycles before compression testing. For torsion testing, a torque of 17 N m was applied on the stem. Moment and direction were chosen according to average moment acting on instrumented hip implants during stair climbing (Bergmann et al., 2010b, 2010a). The bone was preconditioned with 50 torsional load cycles before torsion testing. All tests were performed at room temperature.

#### 2.6. Bias and repeatability estimation

Bias and repeatability were measured in both compression and torsion to evaluate the technique reliability. The bias (a measure of the difference between the average of measurements made on the same object and its true value) was

estimated by measuring micromotion between three pairs of successive unloaded scans (Fig. 3). Each 3D component of micromotion followed a normal distribution, with mean 0. The bias was defined as the 95% confidence interval (95% CI) of micromotion measurement, corresponding to  $\pm 1.96^*SD$ , where SD is the standard deviation of micromotion pooled over the three pairs of measurement.

To estimate repeatability, micromotion measurements in compression and torsion were repeated three times (Fig. 3), under repeatability conditions (same laboratory, same operator, same apparatus, and all tests performed on the same day). Corresponding markers were matched between the three pairs of measurements. The repeatability standard deviation (sr) was calculated as the pooled standard deviation of repeated measurements. The 95% repeatability limit (r) (the maximum difference between two results obtained under repeatability conditions that can be attributed to the test method precision) was defined as  $1.96^*\sqrt{2^*sr}$  according to current ASTM recommendations (ASTM, 2013).

#### 2.7. Data analysis and statistics

For measurement analysis, the femoral stem was divided into three zones: the metaphyseal zone, the middle diaphyseal zone, and the distal diaphyseal zone, similar to the recommendations of Gruen et al. (1979). Normal and tangential micromotion in compression and torsion were compared in each zone with a Mann-Whitney *U* test. For each loading case, micromotion between zones were also compared using the same Mann-Whitney *U* test.

### 3. Results

#### 3.1. Bias and repeatability

Micromotion was simultaneously measured at 313 points on the bone-implant interface for compression and 337 points for torsion. The bias of the method reached a maximum of 5.1  $\mu$ m (Table 1). The bias was consistent between directions as well as between loading cases. The repeatability standard deviation (sr) ranged from 3.1  $\mu$ m to 4.1  $\mu$ m. It was also comparable between directions and loading cases. The repeatability limit reached a maximum of 10.6  $\mu$ m for compression and 11.5  $\mu$ m for torsion.

#### 3.2. Micromotion in compression and torsion

In compression, normal micromotion was below 6  $\mu$ m around 95% of the stem surface but reached 24  $\mu$ m at the tip of the stem (Fig. 4 and Movie 1). Tangential micromotion was higher than normal micromotion and concentrated on the stem's middle and distal diaphyseal zones. In torsion, high micromotion was concentrated on the stem's metaphyseal and middle diaphyseal parts (Fig. 4 and Movie 2).

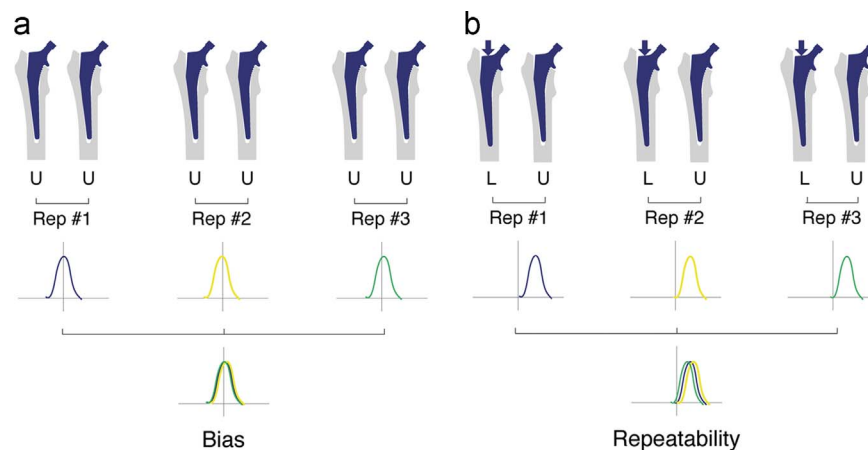


**Fig. 3.** Bias and repeatability estimation protocols. Both protocols were applied successively for compression and torsion. (a) Three pairs of unloaded scans (U) are performed. For each pair of scan (Rep), micromotion is measured. Bias is estimated on these three repeated measurements. (b) Three pairs of unloaded (U) and loaded (L) scans are performed. For each pair of scan (Rep), micromotion is measured. Repeatability is estimated on these three repeated measurements.

Median micromotion was higher in torsion than in compression (Table 2). In compression, micromotion was low proximally and higher distally, whereas in torsion micromotion was high proximally and lower distally. For both loading cases, the differences between micromotion distribution in each zone of the stem was significant. Absolute micromotion was significantly ( $p < 0.0001$ ) higher in torsion than in compression in the metaphyseal and middle diaphyseal zones, while it was significantly lower on the distal diaphysis (Fig. 5).

**Table 1**

Reliability assessment of Micro-CT based measurement of micromotion – values expressed in micrometers. SD: bias standard deviation; 95% CI: bias 95% confidence interval; sr: repeatability standard deviation; r: repeatability 95% limit.

	Bias		Repeatability	
	SD	95% CI	sr	r
<b>Compression</b>				
Lateral to medial	2.4	4.7	3.2	9.0
Anterior to posterior	2.6	5.1	3.8	10.6
Inferior to superior	1.9	3.7	3.1	8.7
<b>Torsion</b>				
Lateral to medial	2.4	4.7	3.9	10.9
Anterior to posterior	2.4	4.7	4.0	11.2
Inferior to superior	1.9	3.7	4.1	11.5

#### 4. Discussion

Micro-CT based techniques such as Digital Volume Correlation (DVC) have been recently used to measure displacement and strain fields in the bone (Roberts et al., 2014). However, extension of micro-CT DVC to measurements at the bone-implant interface faces complications due to artifacts generated by thick metal implants: in consequence of the high atomic number of the metallic implant, the bone would be obscured, streak artefacts would be generated and beam hardening would impact the gray levels at the bone-implant interface (Boas and Fleischmann, 2012). Our aim was to develop a new technique to measure micromotion all around the femur-stem interface, with a bias lower than 10  $\mu\text{m}$  and a good repeatability to allow thorough pre-clinical testing of implants. We proposed a methodology based on radiopaque markers and micro-CT imaging, and measured micromotion around a cementless stem in a cadaveric femur under compressive and torsional loadings. Instead of imaging directly the interface, the radiopaque markers representing the bone and implant surfaces were used. In combination with appropriate scanning parameters, this approach represents the first reported experimental technique leading to a full-field map of interface micromotion around the entire stem.

We tested and compared micromotion values in compression and torsion. We obtained over 300 measurement points spread at the bone-stem interface, and were able to observe local variations of micromotion depending on the loading case. The maximum bias was 5.1  $\mu\text{m}$  and the repeatability limit was 11.5  $\mu\text{m}$ , which demonstrates that the technique is highly reliable. The direction of

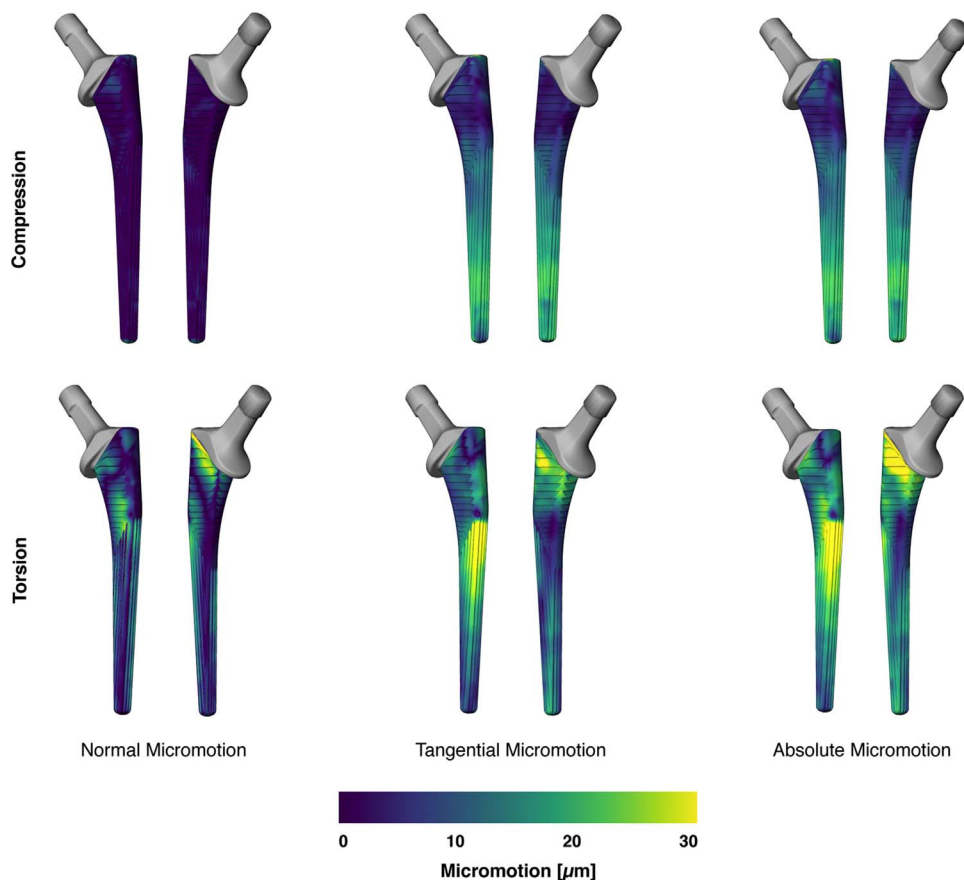
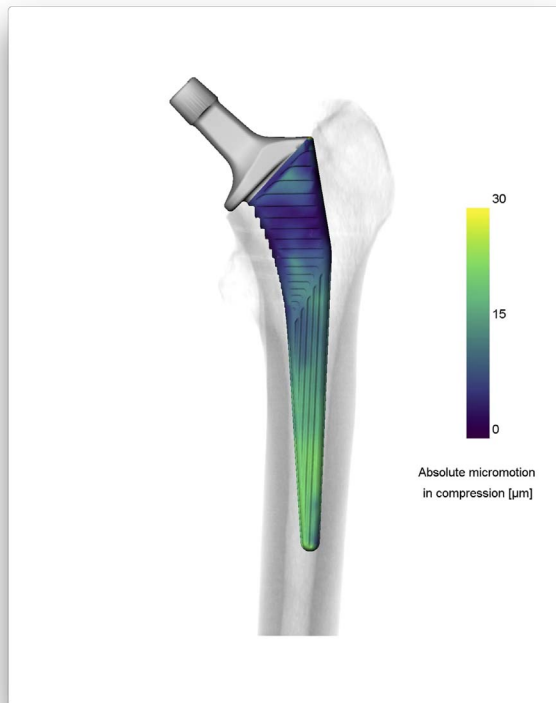


**Fig. 4.** Normal, tangential, and absolute micromotion measured around a cementless femoral stem – Anterior/lateral and posterior/medial views of the stem displayed successively from left to right for each case. Top row shows results obtained in compression. The bottom row shows results obtained in torsion.

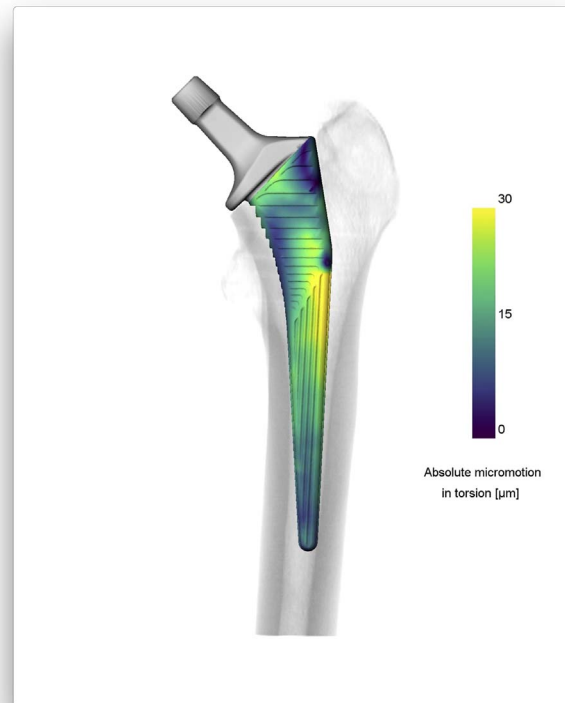


**Video S1.** Full-field absolute micromotion measured at the interface of a cementless femoral stem in compression. 3D volume rendering of the femur from CT data is displayed in gray levels. A video clip is available online. Supplementary material related to this article can be found online at <http://dx.doi.org/10.1016/j.jbiomech.2016.10.029>.

micromotion was distinctly inferior for compression, which is consistent with the axial compressive loading applied. In torsion, normal and tangential micromotion were both comparable in amplitude, in good agreement with an axial torsion of the stem. The stem used in this study is designed to achieve metaphyseal fixation, and consistently, bone-implant gap was particularly low in this zone (Fig. S1 and Movie 3). The metaphyseal region corresponded indeed to a region of low micromotion in compression, but we observed high micromotion in torsion. Generally speaking, there did not seem to be a direct visual correspondence between local bone-implant gap and micromotion.

Supplementary material related to this article can be found online at <http://dx.doi.org/10.1016/j.jbiomech.2016.10.029>.

The validity of the rigid body assumption for the implant has been rigorously verified by calculating the root mean square error (RMSE) of the rigid body registration. The RMSE was approximately  $3\ \mu\text{m}$ , negligible compared to the expected values of interfacial micromotion. Scanning duration was 170 min which is a rather long scanning time. It remained however acceptable, because load relaxation was limited to 1% load loss in compression and 4% in torsion during this time. The fixation of the bone markers was challenging. The markers diameter was chosen to let them penetrate the bone trabeculae, but in the distal medullary canal, cancellous bone is rare. In this region, the markers were simply deposited on the endosteal surface of the bone. Bone markers contiguous to the stem and not well fixed to the bone were a major concern because they could move along with the implant and lead to the underestimation of micromotion. To avoid this issue, the automatic segmentation script removed all bone markers that were in contact with the femoral stem from the measurement. Despite all our efforts, some markers in the



**Video S2.** Full-field absolute micromotion measured at the interface of a cementless femoral stem in torsion. 3D volume rendering of the femur from CT data is displayed in gray levels. Supplementary material related to this article can be found online at <http://dx.doi.org/10.1016/j.jbiomech.2016.10.029>.

**Table 2**

Minimum, maximum, and median micromotion ( $\mu\text{m}$ ) along the different anatomical axis for compression and torsion.

	Min	Max	Median
<b>Compression</b>			
Lateral to medial	-7.8	10.8	1.9
Anterior to posterior	-12	13.7	0.4
Inferior to superior	-24	5.0	12.3
Absolute	0.8	24	13.3
<b>Torsion</b>			
Lateral to medial	-32.5	44.1	-1.5
Anterior to posterior	-42.2	33.8	-7.5
Inferior to superior	-7.8	15.2	0.8
Absolute	2.4	48.7	20.9

metaphyseal area did not enter bone trabeculae and were in direct contact with both the bone and the implant. This situation modifies the original interface and can have an impact on the measurement. However, our results were compatible with measurements obtained with LVDTs. This encourages us to think that this modification of the interface does not change dramatically the magnitude of micromotion. With our method, the distal femur was cemented at approximately half the length of the femur (i.e. at the level of the isthmus) for both loading cases, which is not representative of the actual constraints on the bone and modifies the stress and strain distributions in the femur. However, we were limited by the size of our micro-CT scanner and moving the constraint further away was impossible. For the same reason, the compressive loading was applied on the stem extraction threaded hole of the stem shoulder instead of the implant neck and axial

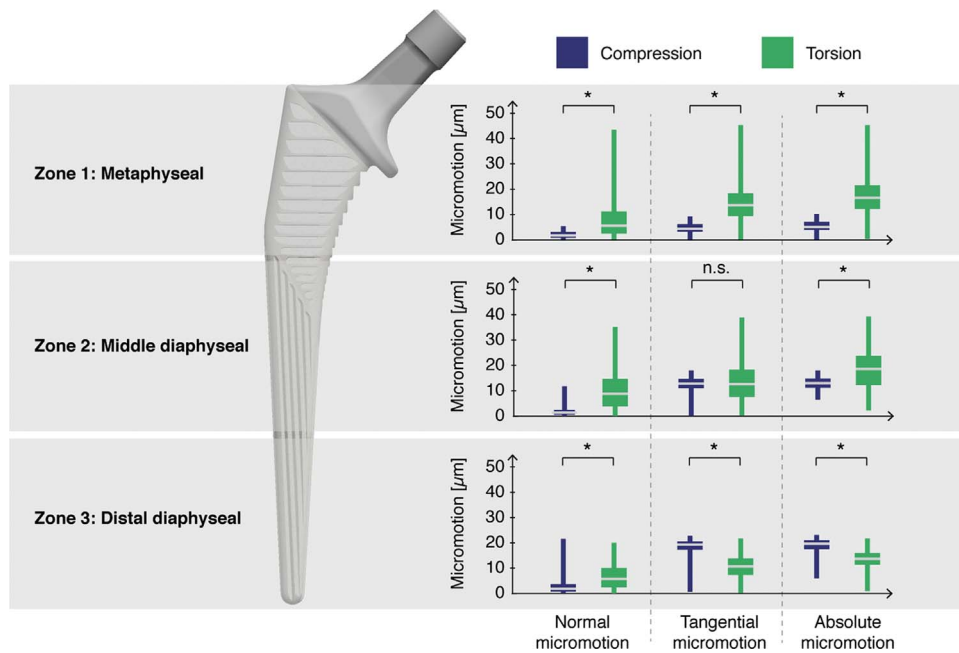


**Fig. 5.** Distribution of normal, tangential, and absolute micromotion in compression and torsion by zone of the femoral stem. Box plots show median value (white line), 1st and 3rd quartiles (bottom and top of the box), and minimum and maximum values (whiskers). Stars (\*) indicate significant difference between pairs of distributions ( $p$ -value < 0.0001).

compression and torsion were tested separately, which does not represent a physiological loading of the stem. Finally, this study was limited to one formalin-fixed femur, for which the mechanical properties are degraded compared to a fresh bone (Currey et al., 1995; Öhman et al., 2008; Stefan et al., 2010). Nevertheless, this allowed us to demonstrate the feasibility of the technique, while avoiding tissue degradation which would have emerged with a fresh frozen bone during the multiple tests conducted in this study.

In general, our results were in good agreement with results reported in the literature. We measured absolute micromotion values that ranged from 0 to 40  $\mu\text{m}$ . Pettersen et al. (2009) measured micromotion in the same range using LVDTs around straight cementless stems in fresh-frozen femurs. Similarly, Abdul-Kadir et al. (2008) measured micromotion of up to 20  $\mu\text{m}$  with LVDTs for an axial compression on the stem shoulder, which is identical to our results. We found higher micromotion in torsion (stair climbing) than in compression (walking). This result compares well with results from Enoksen et al. (2014) and Kassi et al. (2005) obtained with LVDTs or with measurements from postmortem retrieval sections by Mann et al. (2012). The patterns of micromotion revealed that for axial compression, micromotion was low proximally and high distally. Pancanti et al. (2003) observed a similar pattern with a FE model. Moreover, this finding is consistent with the femoral stem design, thought to achieve stabilization in the metaphyseal area (Vidalain, 2010). In torsion, we found high micromotion proximally and lower micromotion distally. Kassi et al. (2005) and Pancanti et al. (2003) also measured higher micromotion proximally but they had a second region of high micromotion at the tip of the stem. Differences in loading and constraints can be possible explanations for this variation.

The reliability of the method was evaluated through bias and repeatability. Maximum bias was 5.1  $\mu\text{m}$ . Although this value is high compared to the accuracy that can be obtained with LVDTs, it remains sufficient to be used for the validation of FE models or for comparing different stems designs. The repeatability standard deviation reached a maximum of 4.1  $\mu\text{m}$ . This value encompasses random errors due to the precision of loading, to the transmission

of load to the femoral stem, and to the viscoelastic behavior of bone. It can be compared to similar measures of repeatability performed for LVDTs setups: Monti et al. (1999) obtained a maximum value of 5  $\mu\text{m}$  for intra-specimen standard deviation, Viceconti et al. (2000) measured a maximum intra-specimen variability of 9  $\mu\text{m}$ , while Kassi et al. (2005) and Østbyhaug et al. (2010) got values of 3  $\mu\text{m}$  and 1.65  $\mu\text{m}$  respectively for repeatability standard deviation. The repeatability of micro-CT based micromotion measurement is thus similar to the repeatability of LVDT-based micromotion measurement.

The technique we proposed here relies on radiopaque markers with different radiopacity and size attached to the bone and the implant to overcome the difficulty of imaging directly the bone-implant interface. The bias and repeatability of the technique were comparable to those of LVDT-based measurements, making it a technique as reliable as the current gold standard. This resulted in a unique full-field map of micromotion around a cementless femoral stem, that may be used to compare the local effects of different implant designs or to corroborate FE results. Notably, the validation of patient-specific models that predict the level of bone-implant micromotion may be a promising application of the proposed technique. Indeed, a validated model could be used for pre-operative planning to compare the performance of different stem designs, of different surgical techniques, or of different stem positions for a given patient. This may improve our understanding of primary implant stability and may lead to enhanced long-term success of cementless total hip arthroplasty.

#### Conflict of interest

None of the authors has any conflict of interest.

#### Acknowledgements

This work was supported by the Swiss National Science Foundation (#141152) and the SwissLife Jubiläumstiftung. The authors

would like to thank DePuy Synthes (DePuy Synthes Joint Reconstruction, Warsaw, IN, USA) for donating the femoral stem and providing CAD files, the Lausanne University Hospital (CHUV) for providing the cadaveric femur, and Alejandro Dominguez and the Centre Universitaire Romand de Médecine Légale (CURML) for the CT-scans of the femur.

## Appendix A. Supplementary material

Supplementary data associated with this article can be found in the online version at <http://dx.doi.org/10.1016/j.jbiomech.2016.10.029>.

## References

- Abdul-Kadir, M.R., Hansen, U., Klabunde, R., Lucas, D., Amis, A., 2008. Finite element modelling of primary hip stem stability: the effect of interference fit. *J. Biomech.* 41, 587–594.
- ASTM, 2013. Standard practice for use of the terms precision and bias in ASTM test methods. In: E177 ed: Subcommittee E11.20 on Test Method Evaluation and Quality Control. ASTM International, West Conshohocken.
- Australian Orthopaedic Association National Joint Replacement Registry, 2015. Annual Report. AOA, Adelaide.
- Bah, M.T., Shi, J., Heller, M.O., Suchier, Y., Lefebvre, F., Young, P., King, L., Dunlop, D. G., Boettcher, M., Draper, E., Browne, M., 2015. Inter-subject variability effects on the primary stability of a short cementless femoral stem. *J. Biomech.* 48, 1032–1042.
- Bergmann, G., Graichen, F., Rohlmann, A., Bender, A., Heinlein, B., Duda, G.N., Heller, M.O., Morlock, M.M., 2010a. Realistic loads for testing hip implants. *Bio-Med. Mater. Eng.* 20, 65–75.
- Bergmann, G., Graichen, F., Rohlmann, A., Bender, A., Heinlein, B., Duda, G.N., Heller, M.O., Morlock, M.M., 2010b. Realistic loads for testing hip implants. *Bio-Med. Mater. Eng.* 20, 381.
- Besl, P.J., McKay, N.D., 1992. A Method for Registration of 3-D Shapes. *IEEE Trans. Pattern Anal. Mach. Intell.* 14, 239–256.
- Boas, F.E., Fleischmann, D., 2012. CT artifacts: causes and reduction techniques. *Imaging Med.* 4, 229–240.
- Currey, J.D., Brear, K., Zioupos, P., Reilly, G.C., 1995. Effect of formaldehyde fixation on some mechanical properties of bovine bone. *Biomaterials* (16), 1267–1271.
- Engh, C.A., O'Connor, D., Jasty, M., McGovern, T.F., Bobyn, J.D., Harris, W.H., 1992. Quantification of implant micromotion, strain shielding, and bone resorption with porous-coated anatomic medullary locking femoral prostheses. *Clin. Orthop. Relat. Res.* (285), 13–29.
- Enoksen, C.H., Gjerdet, N.R., Klaksvik, J., Arthursson, A.J., Schnell-Husby, O., Wik, T. S., 2014. Initial stability of an uncemented femoral stem with modular necks. An experimental study in human cadaver femurs. *Clin. Biomech.* 29, 330–335.
- Fottner, A., Schmid, M., Birkenmaier, C., Mazoochian, F., Plitz, W., Jansson, V., 2009. Biomechanical evaluation of two types of short-stemmed hip prostheses compared to the trust plate prosthesis by three-dimensional measurement of micromotions. *Clin. Biomech.* 24, 429–434.
- Gortchacow, M., Wettstein, M., Pioletti, D.P., Müller-Gerbl, M., Terrier, A., 2012. Simultaneous and multisite measure of micromotion, subsidence and gap to evaluate femoral stem stability. *J. Biomech.* 45, 1232–1238.
- Gortchacow, M., Wettstein, M., Pioletti, D.P., Terrier, A., 2011. A new technique to measure micromotion distribution around a cementless femoral stem. *J. Biomech.* 44, 557–560.
- Gruen, T.A., McNeice, G.M., Amstutz, H.C., 1979. "Modes of failure" of cemented stem-type femoral components: a radiographic analysis of loosening. *Clin. Orthop. Relat. Res.*, 17–27.
- Kassi, J.-P., Heller, M.O., Stoeckle, U., Perka, C., Duda, G.N., 2005. Stair climbing is more critical than walking in pre-clinical assessment of primary stability in cementless THA in vitro. *J. Biomech.* 38, 1143–1154.
- Leys, C., Ley, C., Klein, O., Bernard, P., Licata, L., 2013. Detecting outliers: do not use standard deviation around the mean, use absolute deviation around the median. *J. Exp. Social. Psychol.* 49, 764–766.
- Mann, K.A., Miller, M.A., Costa, P.A., Race, A., Izant, T.H., 2012. Interface Micromotion of Uncemented Femoral Components from Postmortem Retrieved Total Hip Replacements. *J. Arthroplast.* 27, 238–245.
- Monti, L., Cristofolini, L., Viceconti, M., 1999. Methods for quantitative analysis of the primary stability in uncemented hip prostheses. *Artif. Organs* 23, 851–859.
- Öhman, C., Dall'Ara, E., Baleani, M., Jan, S.V.S., Viceconti, M., 2008. The effects of embalming using a 4% formalin solution on the compressive mechanical properties of human cortical bone. *Clin. Biomech.* 23, 1294–1298.
- Pancanti, A., Bernakiewicz, M., Viceconti, M., 2003. The primary stability of a cementless stem varies between subjects as much as between activities. *J. Biomech.* 36, 777–785.
- Pettersen, S.H., Wik, T.S., Skallerud, B., 2009. Subject specific finite element analysis of implant stability for a cementless femoral stem. *Clin. Biomech.* 24, 480–487.
- Pilliar, R.M., Lee, J.M., Maniopoulos, C., 1986. Observations on the Effect of Movement on Bone Ingrowth into Porous-Surfaced Implants. *Clin. Orthop. Relat. Res.* (208), 108–113.
- Reggiani, B., Cristofolini, L., Varini, E., Viceconti, M., 2007. Predicting the subject-specific primary stability of cementless implants during pre-operative planning: preliminary validation of subject-specific finite-element models. *J. Biomech.* 40, 2552–2558.
- Roberts, B.C., Perilli, E., Reynolds, K.J., 2014. Application of the digital volume correlation technique for the measurement of displacement and strain fields in bone: a literature review. *J. Biomech.* 47, 923–934.
- Stefan, U., Michael, B., Werner, S., 2010. Effects of three different preservation methods on the mechanical properties of human and bovine cortical bone. *Bone* 47, 1048–1053.
- Sukjamsri, C., Geraldes, D.M., Gregory, T., Ahmed, F., Hollis, D., Schenk, S., Amis, A., Emery, R., Hansen, U., 2015. Digital volume correlation and micro-CT: an in-vitro technique for measuring full-field interface micromotion around polyethylene implants. *J. Biomech.* 48, 3447–3454.
- Søballe, K., Brockstedt-Rasmussen, H., Hansen, E.S., Bünger, C., 2009. Hydroxyapatite coating modifies implant membrane formation. *Acta Orthop. Scand.* 63, 128–140.
- Taylor, M., Prendergast, P.J., 2015. Four decades of finite element analysis of orthopaedic devices: where are we now and what are the opportunities? *J. Biomech.* 48, 767–778.
- van der Ploeg, B., Tarala, M., Homminga, J., Janssen, D., Buma, P., Verdonchot, N., 2011. Toward a more realistic prediction of peri-prosthetic micromotions. *J. Orthop. Res.* 30, 1147–1154.
- Viceconti, M., Brusi, G., Pancanti, A., Cristofolini, L., 2006. Primary stability of an anatomical cementless hip stem: a statistical analysis. *J. Biomech.* 39, 1169–1179.
- Viceconti, M., Muccini, R., Bernakiewicz, M., Baleani, M., Cristofolini, L., 2000. Large-sliding contact elements accurately predict levels of bone-implant micromotion relevant to osseointegration. *J. Biomech.* 33, 1611–1618.
- Vidalain, J.P., 2010. Twenty-year results of the cementless Corail stem. *Int. Orthop.* 35, 189–194.
- Østbyhaug, P.O., Klaksvik, J., Romundstad, P., Aamodt, A., 2010. Primary stability of custom and anatomical uncemented femoral stems. *Clin. Biomech.* 25, 318–324.